Journal of Atomic, Molecular, Condensed Matter & Nano Physics
Vol. 10, No. 1, pp. 39–51, 2023
ISSN 2582-8215
Published by RGN Publications

http://www.rgnpublications.com

DOI: 10.26713/jamcnp.v10i1.2980

Review Article

Recent Progress on Atomic Spectroscopy of Highly Ionized Ions in Laboratory Plasmas for Fusion Research

S. Morita*[1], T. Oishi[2], L. Zhang[3], C. F. Dong[4], X. L. Huang[5], H. M. Zhang[3] and M. Goto[1]

[1] *National Institute for Fusion Science, Toki 509-5292, Japan*
[2] *Department of Quantum Science and Energy Engineering, Tohoku University, Sendai 980-8579, Japan*
[3] *Institute of Plasma Physics Chinese Academy of Sciences, Hefei 230031, China*
[4] *Department of Physics, Xihua University, Chengdu 610039, China*
[5] *Energy Research Institute, Langfang 065001, China*
***Corresponding author:** morita.shigeru@toki-fs.jp

Received: May 31, 2022 **Accepted:** July 7, 2022

Communicated by: A. Gupta

Abstract. Magnetic dipole forbidden (M1) transitions have been observed for highly ionized Ar, Kr, Mo and Xe ions in LHD. It was found that the M1 transition is observable if the spontaneous emission coefficient is larger than $\sim 10^2\ \mathrm{s}^{-1}$. An intensity ratio of M1 transition to electric dipole (E1) transition was analyzed for F-like TiXIV by assuming the presence of monoenergetic 90 keV protons originated in neutral beams for plasma heating. An effect of 3.52 MeV alpha (He^{2+}) particle collision was also theoretically examined for F-like MoXXXIV and XeXLVI. We found the XeXLVI intensity can be affected by roughly 10% if the alpha particle density is one percent to the electron density. Lα (n = 3-2) transitions of FeXVII-XXIV were observed at 10-18 Å in LHD. Measured intensity ratios among Ne-like FeXVII lines are examined against T_e and n_e, and compared with theoretical values. An influx rate of W^{6+} ions was determined to be $\Gamma_W = 6 \times 10^{11}\ \mathrm{cm}^{-2}\ \mathrm{s}^{-1}$ from the intensity of WVII which was identified at 216.2 Å and 261.4 Å in HL-2A. Densities of W^{43+} and W^{45+} ions were analyzed and found to be an order of $10^8\ \mathrm{cm}^{-3}$ based on the radial profile measurement of WXLIII-XLVI at 120-134 Å in EAST. Several tungsten spectra from low ionization stages, WIV-VII, were identified in LHD at VUV range of 500-1500 Å and the ion temperature was determined from the Doppler broadening, e.g. T_i(WVI)=137±52 eV.

Keywords. VUV spectroscopy, EUV spectroscopy, Highly ionizes ions

PACS. 52.25.Vy, 52.70.-m, 32.30.Jc, 32.70.-n

1. Introduction

The tungsten material is considered most appropriate for the divertor component in a next-generation deuterium-tritium fueled fusion device of ITER tokamak. Therefore, the study on tungsten atom/ion behaviors became extremely important in ongoing fusion devices. The tungsten behavior has been studied in many fields of the fusion research such as edge and core impurity transports, divertor physics and plasma-wall interaction in addition to physical properties of the solid tungsten. Accurate knowledges on the tungsten spectra and atomic database necessary for the spectral analysis, e.g. spectral structure, photon emission coefficient and wavelength of spectral lines, are also important for reliable diagnostics on the tungsten behavior. Although lots of efforts have been already done on the tungsten spectroscopy not only in the fusion device [1,2] but also in the atomic physics device like EBIT [3,4], the understanding of the tungsten spectra and the construction of the atomic database are still insufficient. Then, the tungsten spectra have been energetically studied in LHD (NIFS at Toki), EAST (ASIPP at Hefei) and HL-2A (SWIP at Chengdu) toroidal devices for magnetic-confinement fusion research. In this paper, recent progresses in these devices on the tungsten study are reported in addition to studies on the M1 and Lα transitions of high-Z ions.

2. Spatial Distribution of Impurity Ions

In the toroidal plasma for fusion research the toroidal magnetic field lines with poloidal pitch angles create magnetic surfaces for the plasma confinement of high-temperature plasma. The plasma pressure is constant along the magnetic surface. The magnetic surface in LHD is indicated in Figure 1(a) with ten elliptical contours plotted inside the last-closed flux surface (LCFS) [5]. In general, the T_e has a peaked profile, e.g. $T_e(\rho) = T_e(0)(1-\rho^2)$, while the n_e can change the profile, e.g. peaked, flat and hollow profiles. Here, $T_e(0)$ and ρ denote the central electron temperature and normalized plasma radius ($\rho = r/a_p$, r: radial position, a_p: plasma radius at LCFS), respectively. Then, radial positions of $\rho = 0$ and 1 mean plasma center and edge boundary of the core plasma, respectively. On the other hand, the edge plasma existing outside the core plasma is maintained by open magnetic field lines with two- or three-dimensional (3-D) magnetic field structure. In particular, the edge magnetic field in LHD has a full 3-D structure, called stochastic magnetic field layer, as shown in Figure 1(a), i.e. T_e and n_e have a 3-D structure. Therefore, resultant radial profiles of impurity line emissions also reflect the 3-D magnetic field structure. As shown in Figure 1(b), the radial profiles of CIII and CIV emitted from the edge plasma are entirely asymmetric, while those of CVI and WXXVIII emitted from the core plasma within LCFS are symmetric as a function of ρ. In this review, spectra emitted from the core plasma are only represented because the radial profile analysis is straightforward based on the magnetic surface structure. The analysis of the edge impurity emissions needs a help of 3-D edge plasma transport simulation code due to no applicability of Abel inversion method.

3. Magnetic Dipole (M1) Forbidden Transitions

The time-dependent unperturbed Schrödinger equation is solved by

$$i\hbar\frac{\partial\Psi_k}{\partial t} = H_0\Psi_k\,. \tag{1}$$

The equation can be replaced by using the time-independent eigenfunction, ψ_k, and eigenvalues, E_k,

$$\Psi_k = \psi_k(\mathbf{r})\exp(-iE_kt/\hbar), \tag{2}$$

where ψ_k is the sum over the set of eigenfunctions. Introducing the external vector potential, the transition matrix element is defined as

$$\langle\psi_b|\exp(i\mathbf{k}\cdot\mathbf{r})\hat{\varepsilon}\cdot\nabla|\psi_a\rangle, \tag{3}$$

where $\hat{\varepsilon}$ is the unit vector for polarization of radiation and $\mathbf{k}$ the propagation vector of radiation. Subscripts of a and b mean the initial and final states of the transition, respectively. The exponential term of $\exp(i\mathbf{k}\cdot\mathbf{r})$ can be thus expanded as

$$\exp(i\mathbf{k}\cdot\mathbf{r}) = 1 + (i\mathbf{k}\cdot\mathbf{r}) + \frac{1}{2!}(i\mathbf{k}\cdot\mathbf{r})^2 + \cdots. \tag{4}$$

If the quantity of kr (k: wave number, r: atomic size) is small, e.g. $kr = 10^{-3} \sim 10^{-4}$ in general atoms, the left-hand side exponential can be replaced by unity. This is well known as the electric dipole (E1: $\Delta\ell = \pm1$) transition, and has been generally observed in the plasma spectroscopy. Because the magnetic interaction is much smaller than the electric interaction for ions in low and medium atomic numbers. However, if the higher terms in the right-hand side series is not negligible in increasing the nuclear potential energy, it allows the magnetic dipole (M1: $\Delta n = 0$ and $\Delta\ell = 0$) and electric quadrupole (E2: $\Delta\ell = 0, \pm2$) transitions. Increasing the atomic number, Z, the intensity of the forbidden transition like M1 becomes strong due to a breaking of L-S coupling based on a large enhancement of the relativistic effect such as spin-orbit interaction.

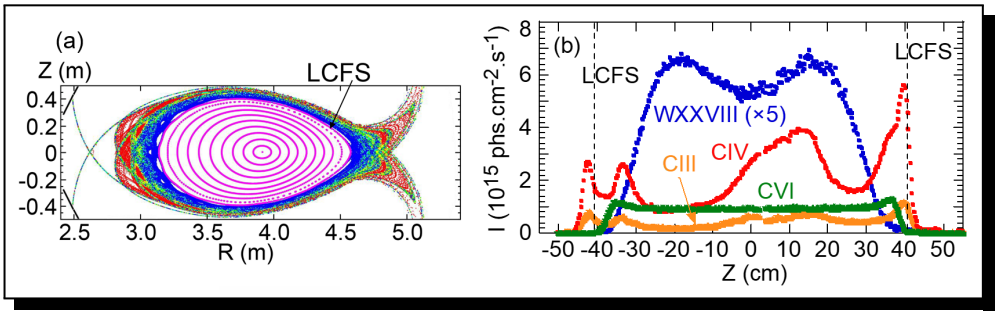

Figure 1. (a) Plasma cross section of LHD, and (b) radial profiles of CIII (386.2 Å), CIV (384.2 Å), CVI (33.7 Å) and WXXVIII (47.8-48.3 Å) along vertical Z direction. Last closed flux surface (LCFS) means a boundary between edge and core plasmas

4. Observations of M1 Transitions and Contribution of High-Energy Ion Collision

Ar discharges were carried out in LHD to observe M1 spectra [6]. Two visible M1 transitions of ArX ($2s^22p^5\ ^2P_{3/2}$-$^2P_{1/2}$: 5533Å) and ArXV ($2s2p\ ^3P_1$-$^3P_2$: 5944Å) are shown in Figure 2(a). The two M1 transitions are completely isolated from other lines. The F-like ArX M1 transition

can be used for the intensity analysis compared to the resonance transition of ArX ($2s^2 2p^5\ ^2P_{3/2}$-$2s2p^6\ ^2S_{1/2}$) at 165.53 Å. The M1 transitions from highly ionized Kr, Mo and Xe ions were also observed in LHD [7] by injecting inert gas or a solid impurity pellet [8]. Typical spectra are shown in Figures 2(b)-(d). In general, identification of the M1 transition from highly ionized ions in such heavy elements is easy because the spectral line is broadened due to the high ion temperature, as clearly seen in Figure 2(d) with M1 and E1 transitions. Another good method for finding the M1 transition is to use the polarization effect. The σ and π components of the M1 line show entirely an opposite direction to the magnetic field line against the E1 line [9].

Wavelengths determined in the present work is plotted in Figure 2(e) as a function of atomic number. The wavelengths are in good agreement with Hatree-Fock approach [10] which includes semi-empirical relativistic corrections based on several experimental results. In particular, the wavelength of Ar M1 transition shows an excellent agreement with the theoretical value because the LS-coupling is still applicable to the Ar ions [11]. Attempts to observe the Ti-like WLIII (W^{52+}: E_i=4.93 keV) failed due to a lack of sufficient electron temperature. The spontaneous emission coefficient, A, is shown in Figure 2(f) for F-, Si- and Ti-like M1 transitions. From the figure we found the M1 line emission can be detected when the A value of the M1 transition ranges in $10^2 \le A \le 10^3\ s^{-1}$.

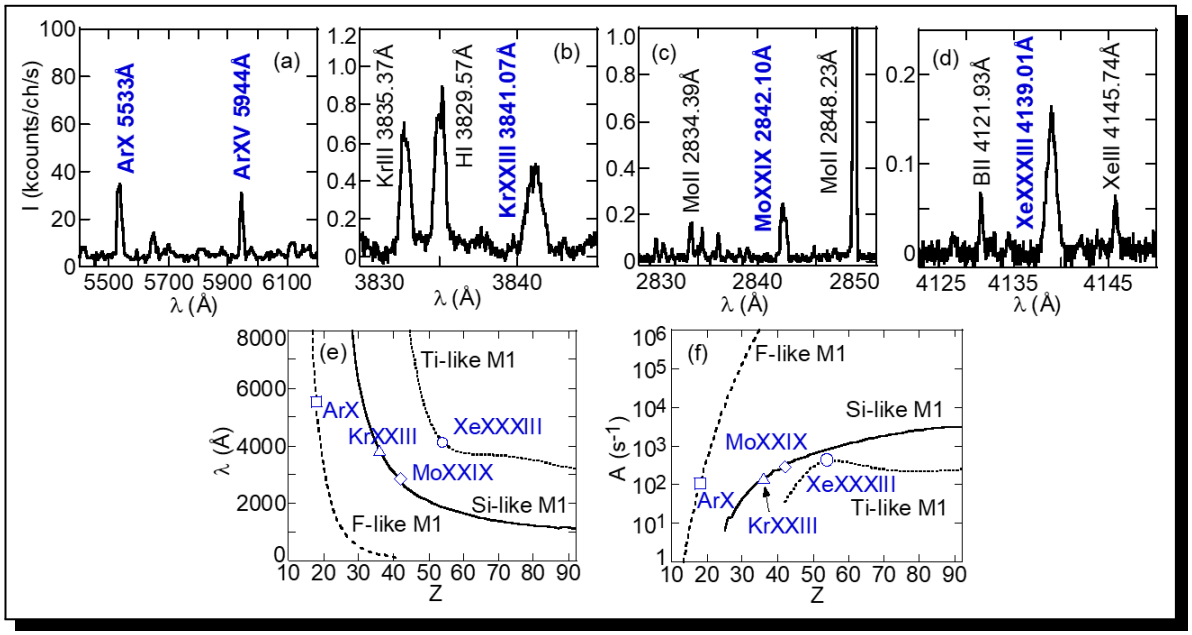

Figure 2. M1 spectra of (a) Be- and F-like Ar, Si-like (b) Kr and (c) Mo and (d) Ti-like Xe, and (e) wavelengths and (f) spontaneous emission coefficients of M1 transitions against atomic number

The study of M1/E1 line intensity ratio is interesting because the ratio depends on not only the collision by thermal electrons but also the collision by high-energy ions [11]. The F-like ion with relatively simple atomic configuration, i.e. single electron vacancy at the outermost orbit, was selected for the present study. The energy level diagram of F-like TiXIV is illustrated in Figure 3(a). The width of arrows represents the magnitude of the population flow at a temperature range where the Ti^{13+} ion exists. The population at level 3 proportionally increases against the electron density, since the population at level 1 follows the corona equilibrium. On

the other hand, the population mechanism at level 2 is complicated because the spontaneous transition probability of level 2 is extremely small.

Five processes are considered for the analysis of the level 2 population, i.e., electron- (EI) and proton-impact (PI) excitations and de-excitations, electron-impact ionization (EI) and E1 and M1 radiative decays (RD). A set of quasi-steady-state rate equations for the F-like ion is written by

$$n_1 = n_{g1}, \tag{5}$$

$$n_2[n_e(C^e_{21}+C^e_{23}+S_2)+n_pC^p_{21}+n_{fp}C^{fp}_{21}+A_{21}] = n_1(n_eC^e_{12}+n_pC^p_{12}+n_{fp}C^{fp}_{12})+n_3(A_{32}+n_eC^e_{32}), \tag{6}$$

$$n_3[n_e(C^e_{31}+C^e_{32}+S_3)+A_{31}+A_{32}] = n_1n_eC^e_{13}+n_2n_eC^e_{23}, \tag{7}$$

where the subscripts of 1, 2, and 3 are denoted in Figure 3(a) and the value of n_{g1} means the ground state population.

The result from the calculation is shown with solid line in Figure 3(b). The level 2 is mainly populated by two processes of the collisional excitation from level 1 and the radiative cascade from level 3, of which the transition rates are proportional to the electron density. In low-density range, therefore, the ratio of M1/E1 is constant because the level 2 is depopulated through the M1 radiative decay. Increasing the density, the collisional de-excitation at level 2 begins to predominate over the radiative process. The level 2 population then saturates in high-density range. As a result, the line intensity ratio of E1/M1 depends on the density, reflecting the density dependence of E1 transition.

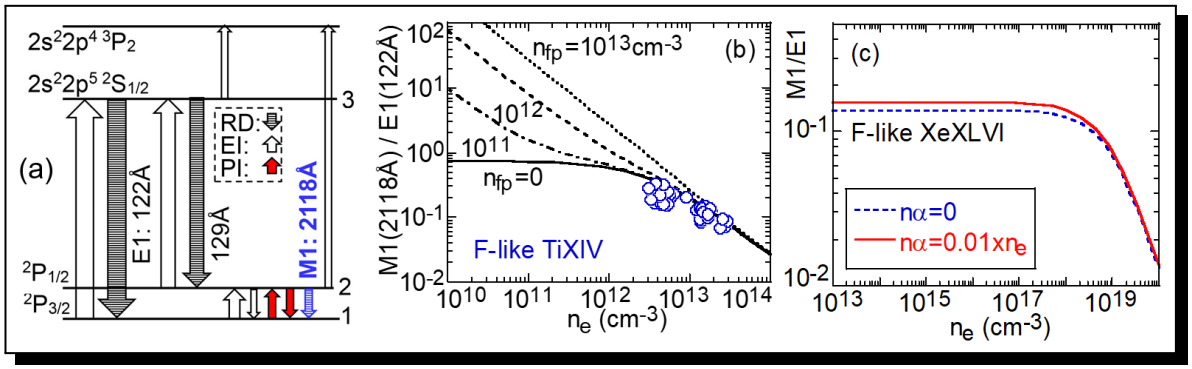

Figure 3. (a) Level diagram for F-like ions, and ratios of F-like M1 to E1 transitions against electron density as a parameter of (b) 90 keV fast ion and (c) 3.52 MeV alpha-particle densities

The collisional excitation by monoenergetic fast protons assumed 90 keV was examined [12]. The value is obtained as an averaged energy of 180 keV hydrogen neutral beam injection (NBI) for plasma heating. The result is also shown in Figure 3(b) as a parameter of fast proton density in range of $0 \le n_{fp} \le 10^{13}$ cm^{-3}. The value of n_{fp} takes 1.4×10^{13} cm^{-3}, if all fast ions injected from NBI are fully confined in the LHD plasma. We understand the ratio of M1/E1 is surprisingly affected by the presence of the fast proton in low density range of $n_e < 10^{12}$ cm^{-3}. Contribution of the fast proton collision disappears in high density range of $n_e > 10^{13}$ cm^{-3} because of an increase in the electron collision excitation. As the LHD NBI discharge operation at $n_e \le 0.2 \times 10^{13}$ cm^{-3} was not possible, a clear experimental certification on

the fast proton collision was unfortunately difficult. However, the TiXIV M1/E1 ratio measured in the experiment (open circles in Figure 3(b)) shows a good agreement with the calculation.

The steady state discharge in a fusion reactor is sustained by an energy dissipation of high-energy α particles (He^4) generated with the following nuclear fusion reaction;

$$D + T \rightarrow He^4\ (3.52\,\mathrm{MeV}) + n\,(14.06\,\mathrm{MeV}). \tag{8}$$

Therefore, information of the α particle created in a next-generation fusion device such as ITER is indispensable in sustaining a high-performance plasma. Here, a possibility for the α particle diagnostic using the M1/E1 intensity ratio is examined. The ion collision cross section calculated with the flexible atomic code (FAC) is extrapolated for heavier ions. In this calculation the α particle is simply assumed to have a monoenergetic distribution. An example of the M1/E1 line ratio calculated for F-like ions is shown for Xe^{45+} ions in Figure 3(c) as a function of electron density. The solid line indicates the calculation assumed 1% α particle density, i.e. $n_\alpha = 0.01 \times n_e$, and 10 keV ion temperature at the plasma center. Contribution of the bulk ion collision is considerably large because the ion temperature is sufficiently high for creating the M1 transition. Nevertheless, the ratio increases by 13% if the α particle exists in the plasma. The Ti-like M1 transition such as WLIII (W^{52+}) is also useful for the α particle diagnostic. At present, however, reliable atomic data calculation does not exist for the Ti-like M1 transition due to the complexity, e.g. existence of 34 fine structure levels in the ground level.

5. Fe Lα (n = 3-2) Transitions

The Ne-like ion is a dominant ionization state in the ionization balance existing over a broad electron temperature range due to the closed L shell atomic configuration. Then, 3s-2p and 3d-2p Lα transitions of Ne-like iron (Fe^{16+}) emitted in wavelength range of 15-17 Å have been extensively studied in both astrophysical and laboratory plasmas including solar and fusion plasmas [13–15]. In particular, the FeXVII lines at 17.097 Å, 17.054 Å and 16.777 Å are useful for measurements of electron temperature and density in addition to the ion abundance analysis. The Fe Lα transitions are also useful for the impurity transport study in fusion plasmas [16]. In spite of the importance, however, observed intensities of a few FeXVII lines have not been well interpreted by the C-R model, e.g. intensity ratio between 3s-2p and 3d-2p transitions and intensity of 3d-2p transition. A further study is necessary for accurate analysis on the intensity of Ne-like FeXVII Lα transitions.

The Fe n = 3-2 Lα transition array composed of ionization stages of Ne-like Fe^{16+} to Li-like Fe^{23+} ions were observed in LHD at wavelength interval of 10-20 Å [17]. A typical spectrum of the Fe Lα array is shown in Figure 4(a). Several FeXVII lines are identified as

3C : 15.015 Å ($2p^5 3d\ ^1P_1 \rightarrow 2p^6\ ^1S_0$),

3D : 15.262 Å ($2p^5 3d\ ^3D_1 \rightarrow 2p^6\ ^1S_0$),

3E : 15.450 Å ($2p^5 3d\ ^3P_1 \rightarrow 2p^6\ ^1S_0$),

3F : 16.777 Å ($2p^5 3s\ ^3P_1 \rightarrow 2p^6\ ^1S_0$),

3G : 17.054 Å ($2p^5 3s\ ^1P_1 \rightarrow 2p^6\ ^1S_0$) and

M2 : 17.097 Å ($2p^5 3s\ ^3P_2 \rightarrow 2p^6\ ^1S_0$).

The 3G line is blended with the M2 line, probably due to a limited spectral resolution. The 3E

line is usually weak. The 3G+M2 and 3C lines exhibit a strong intensity in the Fe Lα transition array. When the electron temperature is low, the Ne-like FeXVII is dominant in the Fe $n = 3$-2 transition array. Lα transitions from higher ionization stages seen in Figure 4(a) are gradually strong when the electron temperature increases.

Radial profiles of the FeXVII Lα lines measured along the vertical direction are plotted in Figure 4(b). In order to analyze the profile data, radial profiles of the local emissivity [photons s^{-1} cm^{-3}] must be derived from the radial intensity profile in Figure 4(b) based on an Abel inversion technique. The magnetic flux surface structure in LHD plasmas is calculated as a parameter of plasma pressure profile. Then, the integral length between adjacent two magnetic surfaces along the observation chord of the spectrometer can be evaluated for the Abel inversion.

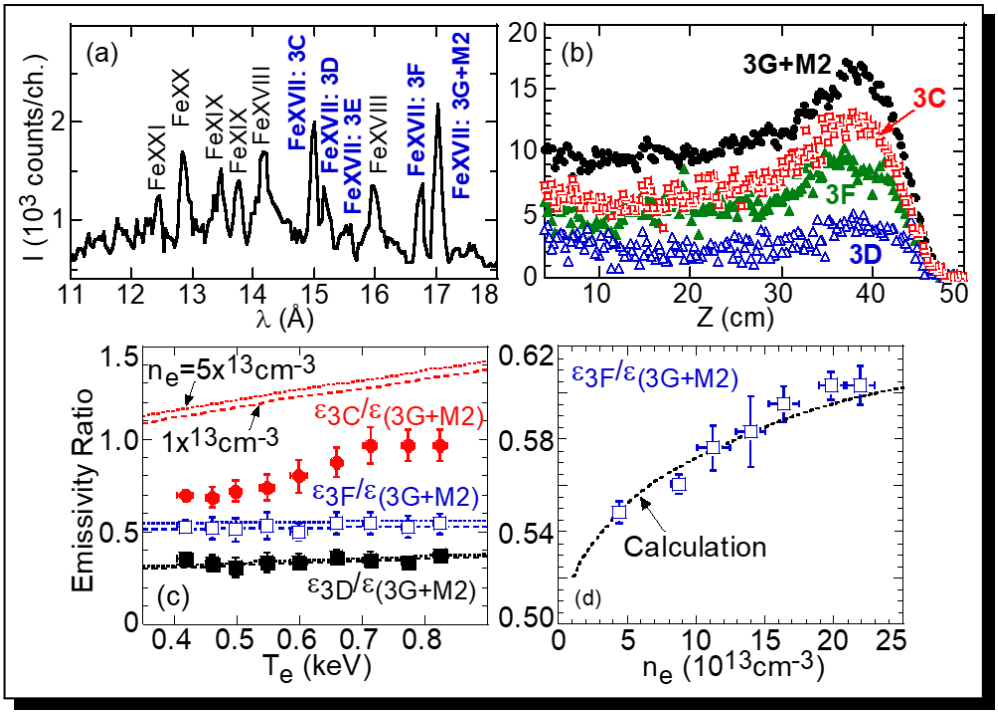

Figure 4. (a) Fe Lα spectrum, (b) radial profiles of Ne-like Fe Lα emissions, and emissivity ratios among Ne-like Fe Lα transitions against (c) electron temperature and (d) density

A CR model was developed for Fe ions including fine-structure levels at principal quantum numbers up to $n = 5$ [18]. Assuming a quasi-steady state, the CR model includes all relevant atomic processes necessary for determining the level population. Most of atomic data are calculated with HULLAC code [19].

The emission coefficients of Fe XVII transitions are calculated with the CR model. The upper level in the 3d-2p transitions (3C, 3D and 3E) is mainly populated through the collisional excitation from the ground level, whereas the upper levels of 3s-2p transitions (3F, 3G and M2) are dominantly populated by the cascade from higher levels. When the electron density increases above 10^{13} cm^{-3}, the 3G and 3F intensities increase with density due to a population redistribution through electron collisions. However, the intensity of the M2 transition decreases with density due to a specific character of the forbidden transition.

Emissivity ratios evaluated at the peak position of radial emissivity profiles are shown in

Figure 4(c) as a function of electron temperature, T_e, with results of the CR model calculation. The experimental result that the emissivity ratios of $\epsilon_{3D}/\epsilon_{(3G+M2)}$ and $\epsilon_{3F}/\epsilon_{(3G+M2)}$ are not sensitive to the electron temperature shows a good agreement with the theoretical prediction. In contradiction to it, the emissivity ratio of $\epsilon_{3C}/\epsilon_{(3G+M2)}$increases with T_e. It is found that the measured ratio is smaller than the theoretical calculation by 25-40%. It seems that the discrepancy in the ratio of $\epsilon_{3C}/\epsilon_{(3G+M2)}$ is attributed to an overestimation of the 3C emissivity.

The present result is entirely consistent with results from solar corona [20], PLT tokamak [15] and EBIT [13, 21]. A recent study on the oscillator strength of 3C/3D suggests that the discrepancy is caused by the accuracy in atomic wave functions [22]. Further improvement is required for the theoretical modeling with accurate treatment on the spin-orbit interaction.

A density effect on the ratio of $\epsilon_{3F}/\epsilon_{(3G+M2)}$ was also studied by analyzing the radial emissivity profile. The result is shown in Figure 4(d) with results of the theoretical calculation. The electron temperature in the analysis is fixed to 0.5 keV where the Ne-like iron exists. The measured ratio agrees well with the theoretical calculation in the density range of $n_e = 4 - 22 \times 10^{13}$ cm^{-3}. The density effect on the FeXVII intensity ratio was thus confirmed through the present study.

6. Influx Rate Analysis from WVII Observed at EUV Region

EUV spectra from low-ionized tungsten ions such as W^{6+} and W^{7+} were recently identified in HL-2A tokamak [23]. Typical W VII and W VIII spectra observed after the tungsten laser-blow-off injection is shown in Figure 5(a). The two W VII lines isolated from other lines are identified with sufficient intensities. Then, the tungsten ion influx rate can be determined from absolute intensity of the W VII line because the W^{6+} ion locates in the plasma edge.

In HL-2A discharges after the laser bow-off injection a sudden enhancement of the plasma-wall interaction sometimes occurs at a divertor plate where the tungsten has been already deposited by the laser blow-off injection. As seen in Figure 5(b), the WVII intensity rapidly increases by the sudden increase in the plasma-wall interaction occurred at $t = 0.842$s.

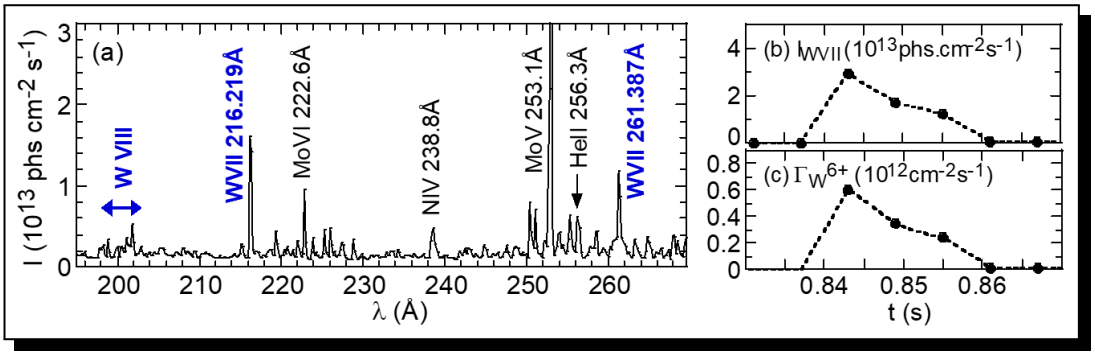

Figure 5. (a) WVIII and WVII spectra, and temporal behaviors of (b) WVII intensity and (c) influx rate of W^{6+} ions

The impurity influx, $\Gamma_{\rm imp}$ (ions$\cdot s^{-1}$ cm^{-2}), for A^{q+} ion can be derived by

$$\Gamma_{\rm imp} = I_{\rm imp} \times (S/XB), \tag{9}$$

where $I_{\rm imp}$ (photons·s^{-1} cm^{-2}) is the measured line intensity, S (cm^{-3} s^{-1}) the electron impact ionization rate, X (cm^{-3} s^{-1}) the electron impact excitation rate and B the branching ratio. The coefficient, S/XB, called 'inverse photon efficiency' denotes the number of ionization events per detected photon (ions/photon). In the present analysis the ADAS code [24] is used for deriving the inverse photon efficiency. The result is shown in Figure 5(c). The total number of W^{6+} ions, N_{W6+}, entering the HL-2A plasma can be obtained by integrating the influx rate over the whole plasma surface, i.e. $N_{W6+} = 1.4 \times 10^{15}$. If all W^{6+} ions are fully confined and uniformly distributed in the plasma, the tungsten density can be roughly estimated to be $n_W \sim 10^9$ cm^{-3}. The value may indicate a reasonable tungsten density of $n_W/n_e \sim 10^{-4}$ to the electron density.

7. Tungsten Density Profile Analysis from WXLIV and WXLVI Radial Profiles

EUV spectra from highly ionized tungsten ions have been energetically studies in EAST tokamak. A typical spectrum with WXLIII-WXLVI is represented in Figure 6(a). Radial intensity profiles of W XLIV (128.29 Å) from W^{43+} ions and W XLVI (126.998 Å) from W^{45+} ions observed during an H-mode phase of the EAST discharge with $T_e = 2.9$ keV are shown in Figure 6(b) [25]. The abscissa is indicated with the normalized plasma radius because the plasma has a vertically elongated D-shaped cross section. To analyze the density profile of tungsten ions the radial intensity profile, I [phs·cm^{-2} s^{-1}], is reconstructed to the local emissivity profile, ϵ [phs·cm^{-3} s^{-1}]. The ion density can be then calculated from an equation of $\epsilon = n_W \times n_e \times f_{\rm PEC}$. Here, the $f_{\rm PEC}$ is the photon emission coefficient, which is taken from the open-ADAS database [24]. The result is plotted in Figure 6(c). The centrally peaked density profiles of W^{43+} and W^{45+} ions indicate that those ions locate in the central plasma region. It is understood that the W^{43+}-W^{45+} densities range in 2-6×10^8 cm^{-3}, i.e. $n_W/n_e \sim 0.2\text{-}0.5 \times 10^{-4}$. The result reveals that the H-mode is still sustainable in such discharges with relatively high tungsten concentration.

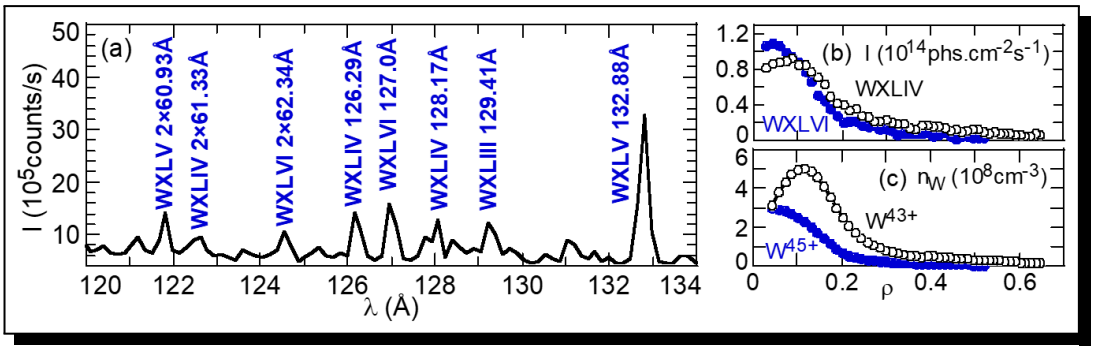

Figure 6. (a) WXLIII-XLVI EUV spectra, and radial profiles of (b) WXLIV and WXLVI intensities and (c) W^{43+} and W^{45+} densities as a function of normalized plasma radius

8. Doppler Profile Measurement of WVI Observed at VUV Region

VUV spectra from low-ionized tungsten ions were observed with a high-resolution 3m normal incidence VUV spectrometer in LHD by injecting a tungsten impurity pellet. The tungsten spectra were identified in the VUV range of 500-1500 Å in detail. As a result, many tungsten lines from W^{3+} to W^{6+} ions were successfully identified [26]. Typical VUV spectrum at the

2nd order light of WVI (2×605.926 Å) is represented in Figure 7(a). Most of the VUV lines measured from LHD plasmas are entirely isolated from other lines because the spectrometer has a sufficiently high spectral resolution and large wavelength dispersion which enable an accurate spectral profile analysis. The WVI spectrum shown in Figure 7(a) is enlarged in Figure 7(b). It clearly exhibits a Doppler-broadened profile with spectral line width of 0.221 Å. The line width gives a local ion temperature of 137eV for the W^{5+} ion.

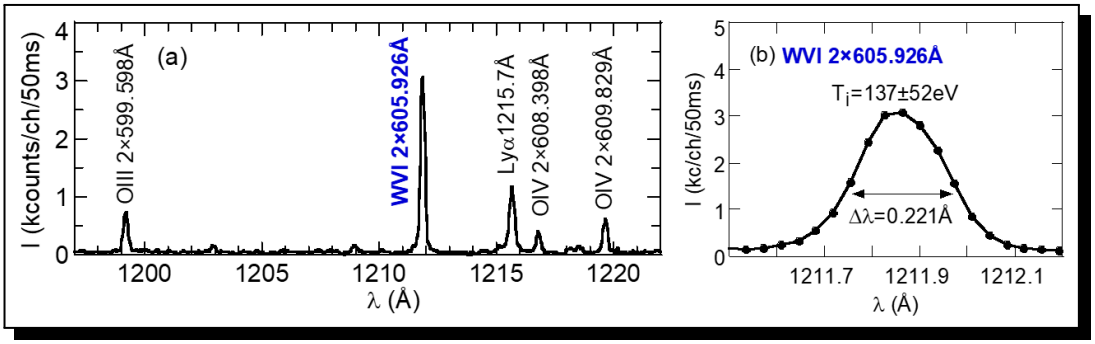

Figure 7. (a) WVI VUV spectrum and (b) Doppler profile of WVI line emission

9. Summary and Future Prospect

A Study of M1 transitions in LHD and application of the M1 transition to alpha particle diagnostics in D-T burning plasmas were reviewed. Recently, the M1 transition was also identified for tungsten W^{26+} ions at 3894 Å and 3899 Å in laboratory plasmas of LHD [27]. Fe Lα transitions were measured at 11-18 Å for the impurity transport study. The intensity ratios among Ne-like FeVII Lα transitions were analyzed, which are useful for diagnostics of astrophysical plasmas. Tungsten influx rate analysis from WVII spectra at 216.2 Å and 261.4 Å in HL-2A tokamak, tungsten density analysis based on radial profiles of WXLIV (126.29 Å) and WXLVI (127.0 Å) spectra in EAST tokamak and Doppler profile analysis of WVI spectrum at 2×605.926 Å in LHD were represented in this review paper.

Further studies of visible and EUV spectra from highly ionized tungsten ions will be progressed in EAST because the LHD operation after 2023 is not guaranteed at present. All graphite divertor plates of EAST have been recently replaced by tungsten divertor plates. We can expect sufficient intensities from tungsten ions basically in all discharges, while an external tungsten particle injection was necessary for tungsten spectroscopy in HL-2A and LHD. Further progress of the tungsten M1 transition study in visible range is extremely important for the tungsten diagnostics in future fusion devices with D-T burning plasmas such as ITER (International Thermonuclear Experimental Reactor in Cadarache) and BEST (Burning plasma Experimental Superconducting Tokamak in Hefei) because the visible light can be easily transferred to another experimental room without neutron and hard x-ray backgrounds. Further studies on the photon emission coefficient of tungsten spectra including an effect of high-energy particle collisions are also very important for fulfilling well-established tungsten diagnostics.

Acknowledgements

This work was partly supported by the LHD collaboration program (NIFS21KLPP069) and JSPS Grants-in-Aid for Scientific Research (KAKENHI: Grant Number 16H04088). The authors wish to thank for Chinese Academy of Sciences President's International Fellowship Initiative (PIFI) (No. 2020VMA001, 2024PVA0074, 2025PVA0060).

Competing Interests

The authors declare that they have no competing interests.

Authors' Contributions

All the authors contributed significantly in writing this article. The authors read and approved the final manuscript.

References

[1] S. Morita, C.F. Dong, D. Kato, Y. Liu, L. Zhang, Z.Y. Cui, M. Goto, Y. Kawamoto, I. Murakami and T. Oishi, Quantitative analysis on tungsten spectra of W^{6+} to W^{45+} ions, *Journal of Physics: Conference Series* **1289** (2019), 012005-1-7, DOI: 10.1088/1742-6596/1289/1/012005.

[2] T. Pütterich, E. Fable, R. Dux, M. O'Mullane, R. Neu and M. Siccinio, Determination of the tolerable impurity concentrations in a fusion reactor using a consistent set of cooling factors, *Nuclear Fusion* **59** (2019), 056013-1-28, DOI: 10.1088/1741-4326/ab0384.

[3] J. Rzadkiewicz, Y. Yang, K. Kozioł, M.G. O'Mullane, A. Patel, J. Xiao, K. Yao, Y. Shen, D. Lu, R. Hutton, Y. Zou and J.E.T. Contributors, High-resolution tungsten spectroscopy relevant to the diagnostic of high-temperature tokamak plasmas, *Physical Review A* **97** (2018), 052501-1-9, DOI: 10.1103/PhysRevA.97.052501.

[4] H.A. Sakaue, D. Kato, N. Yamamoto, N. Nakamura and I. Murakami, Spectra of W^{19+}-W^{32+} observed in the EUV region between 15 and 55 Å with an electron-beam ion trap, *Physical Review A* **92** (2015), 012504-1-6, DOI: 10.1103/PhysRevA.92.012504.

[5] S. Morita, E.H. Wang, M. Kobayashi, C.F. Dong, T. Oishi, Y. Feng, M. Goto, X.L. Huang, S. Masuzaki, I. Murakami, Y. Suzuki, T. Watanabe and the LHD Experiment Group, Two-dimensional study of edge impurity transport in the Large Helical Device, *Plasma Physics and Controlled Fusion* **56** (2014), 094007-1-10, DOI: 10.1088/0741-3335/56/9/094007.

[6] R. Katai, S. Morita and M. Goto, High-resolution VUV spectra of carbon, neon and argon in a wavelength range of 250 to 2300 Å for plasma diagnostics observed with a 3m normal incidence spectrometer in LHD, *Plasma and Fusion Research* **2** (2007), pages 14, DOI: 10.1585/pfr.2.014.

[7] R. Katai, S. Morita and M. Goto, Observation of visible and near-UV M1 transitions from highly charged Kr, Mo and Xe ions in LHD and its prospect to impurity spectroscopy for D-T burning plasmas, *Plasma and Fusion Research* **2** (2007), pages 6, DOI: 10.1585/pfr.2.006.

[8] X.L. Huang, S. Morita, T. Oishi, M. Goto and H.M. Zhang, Coaxial pellets for metallic impurity injection on the large helical device, *Review of Scientific Instruments* **85** (2014), 11E818-1-4, DOI: 10.1063/1.4892440.

[9] A. Iwamae, M. Atake, A. Sakae, R. Katai, M. Goto and S. Morita, Polarization separated Zeeman spectra from magnetic dipole transitions in highly charged argon in the large helical device, *Physics of Plasmas* **14** (2007), 042504-1-8, DOI: 10.1063/1.2714506.

[10] E. Biémont, E. Träbert and C.J. Zeippen, Calculated transition probabilities in highly charged Ti-like ions, *Journal of Physics B: Atomic, Molecular and Optical Physics* **34** (2001), 1941 – 1951, DOI: 10.1088/0953-4075/34/10/309.

[11] R. Katai, S. Morita and M. Goto, Identification and intensity analysis on forbidden magnetic dipole emission lines of highly charged Al, Ar, Ti and Fe ions in LHD, *Journal of Quantitative Spectroscopy and Radiative Transfer* **107**(1) (2007), 120 – 140, DOI: 10.1016/j.jqsrt.2006.12.010.

[12] S. Morita, M. Goto, R. Katai, C.F. Dong, H. Sakaue and H.Y. Zhou, Observation of magnetic dipole forbidden transitions in LHD and its application to burning plasma diagnostics, *Plasma Science and Technology* **12** (2010), 341 – 347, DOI: 10.1088/1009-0630/12/3/19.

[13] G.V. Brown, P. Beiersdorfer, D.A. Liedahl, K. Widmann and S.M. Kahn, Laboratory measurements and modeling of the FeXVII x-ray spectrum, *Astrophysical Journal* **502**(2) (1998), 1015-1026, DOI: 10.1086/305941.

[14] K.J.H. Phillips, C.J. Greer, A.K. Bhatia, I.H. Coffey, R. Barnsley and F.P. Keenan, FeXVII x-ray lines in solar coronal and laboratory plasmas, *Astronomy and Astrophysics* **324** (1997), 381-394, URL: https://adsabs.harvard.edu/pdf/1997A%26A...324..381P.

[15] P. Beiersdorfer, S. von Goeler, M. Bitter and D.B. Thorn, Measurement of the $3\vec{d}\ 2p$ resonance to intercombination line-intensity ratio in neonlike Fe XVII, GeXXIII and SeXXV, *Physical Review A* **64** (2001), 032705-1-6, DOI: 10.1103/PhysRevA.64.032705.

[16] X.L. Huang, S. Morita, T. Oishi, I. Murakami, M. Goto, H.M. Zhang, Y. Liu and The LHD Experiment Group, Formation of impurity transport barrier in LHD plasmas with hollow density profile, *Nuclear Fusion* **57** (2017), 086031-1-6, DOI: 10.1088/1741-4326/aa7920.

[17] X.L. Huang, E.H. Wang, C.F. Dong, S. Morita, T. Oishi, I .Murakami and M. Goto, Radial profiles and emissivity ratio analysis of Ne-like FeXVII n = 3-2 transitions in Large Helical Device, *Journal of the Korean Physical Society* **65** (2014), 1265 – 1269, DOI: 10.3938/jkps.65.1265.

[18] I. Murakami, H.A. Sakaue, N. Yamamoto, D. Kato, S. Morita and T. Watanabe, Analysis of FeXXI spectral lines measured in LHD plasma, *Plasma and Fusion Research* **5** (2010), S2021-1-4, DOI: 10.1585/pfr.5.S2021.

[19] A. Bar-Shalom, M. Klapisch and J. Oreg, HULLAC, an integrated computer package for atomic processes in plasmas, *Journal of Quantitative Spectroscopy and Radiative Transfer* **71**(2-6) (2001), 169 – 188, DOI: 10.1016/S0022-4073(01)00066-8.

[20] A.K. Bhatia and J.L.R. Saba, Resonance scattering of FeXVII x-ray and extreme-ultraviolet lines, *Astrophysical Journal* **563** (2001), 434 – 450, DOI: 10.1086/323688.

[21] J.M. Laming, I. Kink, E. Takacs, J.V. Porto, J.D. Gillaspy, E.H. Silver, H.W. Schnopper, S.R. Bandler, N.S. Brickhouse, S.S. Murray, M. Barbera, A.K. Bhatia, G.A. Doschek, N. Madden, D. Landis, J. Beeman, and E.E. Haller, Emission-line intensity ratios in FeXVII observed with a microcalorimeter on an electron beam ion trap, *The Astrophysical Journal* **545** (2000), L161 – L164, DOI: 10.1086/317876.

[22] S. Bernitt, G.V. Brown, J.K. Rudolph, R. Steinbrügge, A. Graf, M. Leutenegger, S.W. Epp, S. Eberle, K. Kubiček, V. Mäckel, M.C. Simon, E. Träbert, E.W. Magee, C. Beilmann, N. Hell, S. Schippers, A. Müller, S.M. Kahn, A. Surzhykov, Z. Harman, C.H. Keitel, J. Clementson, F.S. Porter, W. Schlotter, J.J. Turner, J. Ullrich, P. Beiersdorfer and J.R. Crespo López-Urrutia, An unexpectedly low oscillator strength as the origin of the FeXVII emission problem, *Nature* **492** (2012), 225 – 228, DOI: 10.1038/nature11627.

[23] C.F. Dong, S. Morita, Z.Y. Cui, P. Sun, K. Zhang, I. Murakami, B.Y. Zhang, Z.C. Yang, D.L. Zheng, L. Feng, Y. Li, B.Z. Fu, P. Lu, Z.B. Shi, Q.W. Yang, M. Xu and X.R. Duan, Evaluation of tungsten influx rate and study of edge tungsten behavior based on the observation of EUV line emissions from W^{6+} ions in HL-2A, *Nuclear Fusion* **59** (2019), 016020-1-13, DOI: 10.1088/1741-4326/aaf084.

[24] A. Foster, *Open-ADAS*, The ADAS Project, Version 2.1, URL: http://open.adas.ac.uk.

[25] L. Zhang, S. Morita, Z. Wu, Z. Xu, X. Yang, Y. Cheng, Q. Zang, H. Liu, Y. Liu, H. Zhang, T. Ohishi, Y. Chen, L. Xu, C. Wu, Y. Duan, W. Gao, J. Huang, X. Gong and L. Hu, A space-resolved extreme ultraviolet spectrometer for radial profile measurement of tungsten ions in the Experimental Advanced Superconducting Tokamak, *Nuclear Instruments and Methods in Physics Research Section A: Accelerators, Spectrometers, Detectors and Associated Equipment* **916** (2019), 169-178, DOI: 10.1016/j.nima.2018.11.082.

[26] T. Oishi, S. Morita, X.L. Huang, H.M. Zhang, M. Goto and and the LHD Experiment Group, Observation of WIV-WVII line emissions in wavelength range of 495-1475Å in the large helical device, *Physica Scripta* **91** (2016), 025602-1-16, DOI: 10.1088/0031-8949/91/2/025602.

[27] D. Kato, M. Goto, S. Morita, I. Murakami, H.A. Sakaue, X.B. Ding, S. Sudo, C. Suzuki, N. Tamura, N. Nakamura, H. Watanabe and F. Koike, Observation of visible forbidden lines from highly charged tungsten ions at the large helical device, *Physica Scripta* **2013**(T156) (2013), 014081-1-3, DOI: 10.1088/0031-8949/2013/T156/014081.